Science Advances

AAAS

advances.sciencemag.org/cgi/content/full/3/4/e1700325/DC1

Supplementary Materials for

Mechanism of Vps4 hexamer function revealed by cryo-EM

Min Su, Emily Z. Guo, Xinqiang Ding, Yan Li, Jeffrey T. Tarrasch, Charles L. Brooks III, Zhaohui Xu, Georgios Skiniotis

Published 14 April 2017, *Sci. Adv.* **3**, e1700325 (2017)
DOI: 10.1126/sciadv.1700325

The PDF file includes:

Other Supplementary Material for this manuscript includes the following:
(available at advances.sciencemag.org/cgi/content/full/3/4/e1700325/DC1)

- movie S1 (.mov format). Molecular dynamic flexible fitting into Vps4 open and closed cryo-EM maps.
- movie S2 (.mov format). Morphing motion between Vps4 open and closed models.

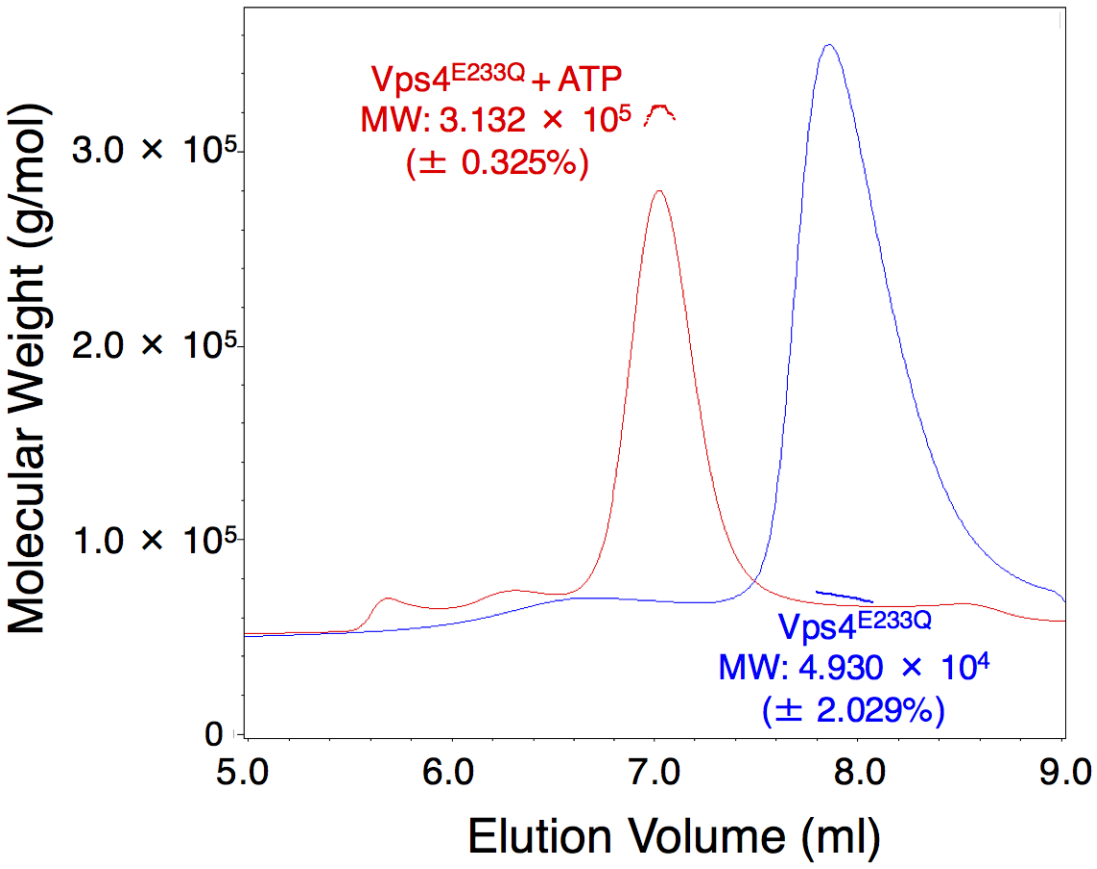

fig. S1. Vps4 oligomerizes into a hexamer in the presence of ATP. Size exclusion chromatography profile of $Vps4^{E233Q}$ in the presence (red curve) and absence of ATP (blue curve). The molecular weights of the species under the elution peak are determined using multi-angle light scattering (MALS) analysis.

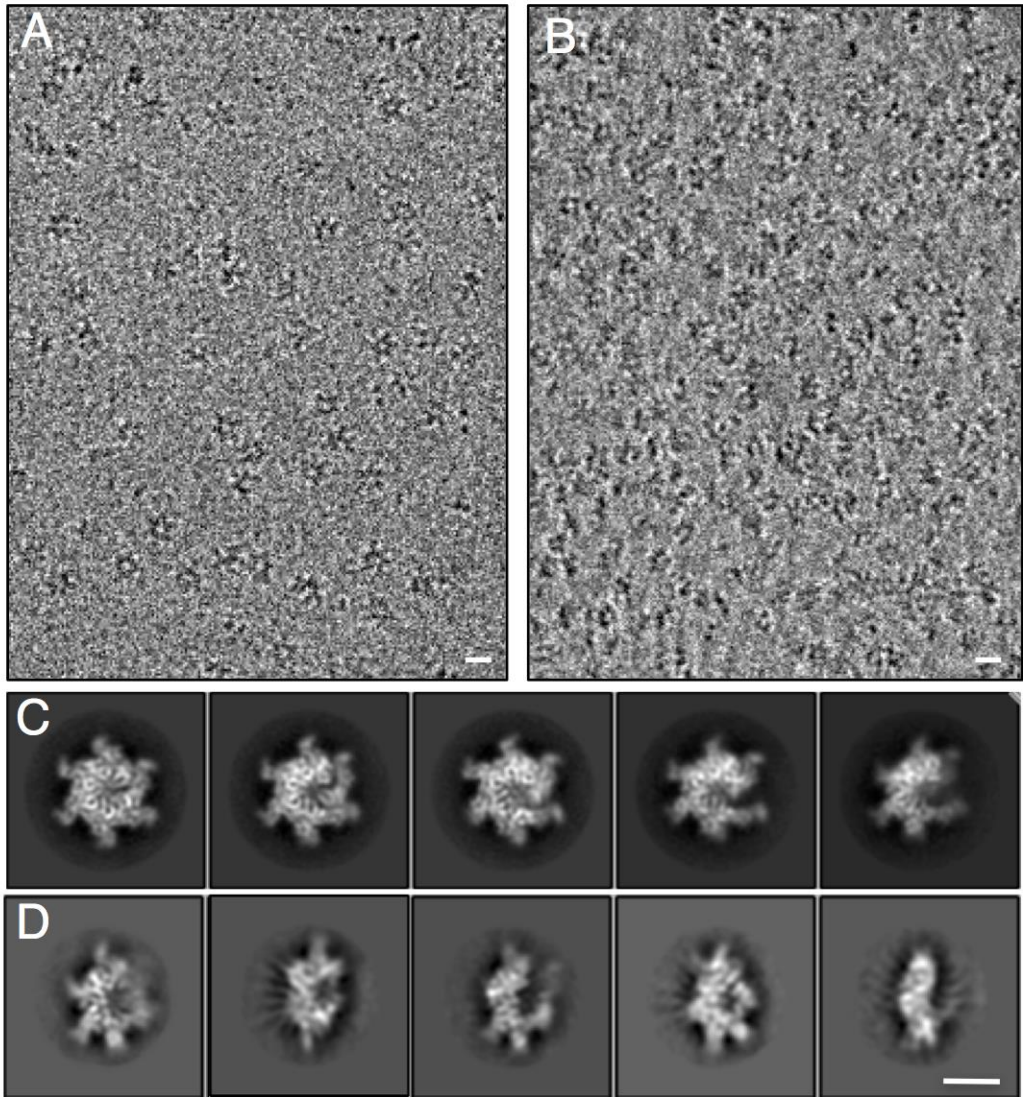

fig. S2. Cryo-EM images of Vps4 oligomer. (**A** and **B**) Representative cryo-EM images of Vps4 oligomer acquired at 0° (A) and 45° (B) tilt. (**C** and **D**) Representative reference-free 2D class averages showing particle projections from 0° (C) and 45° (D) tilt. Scale bar corresponds to 100 Å.

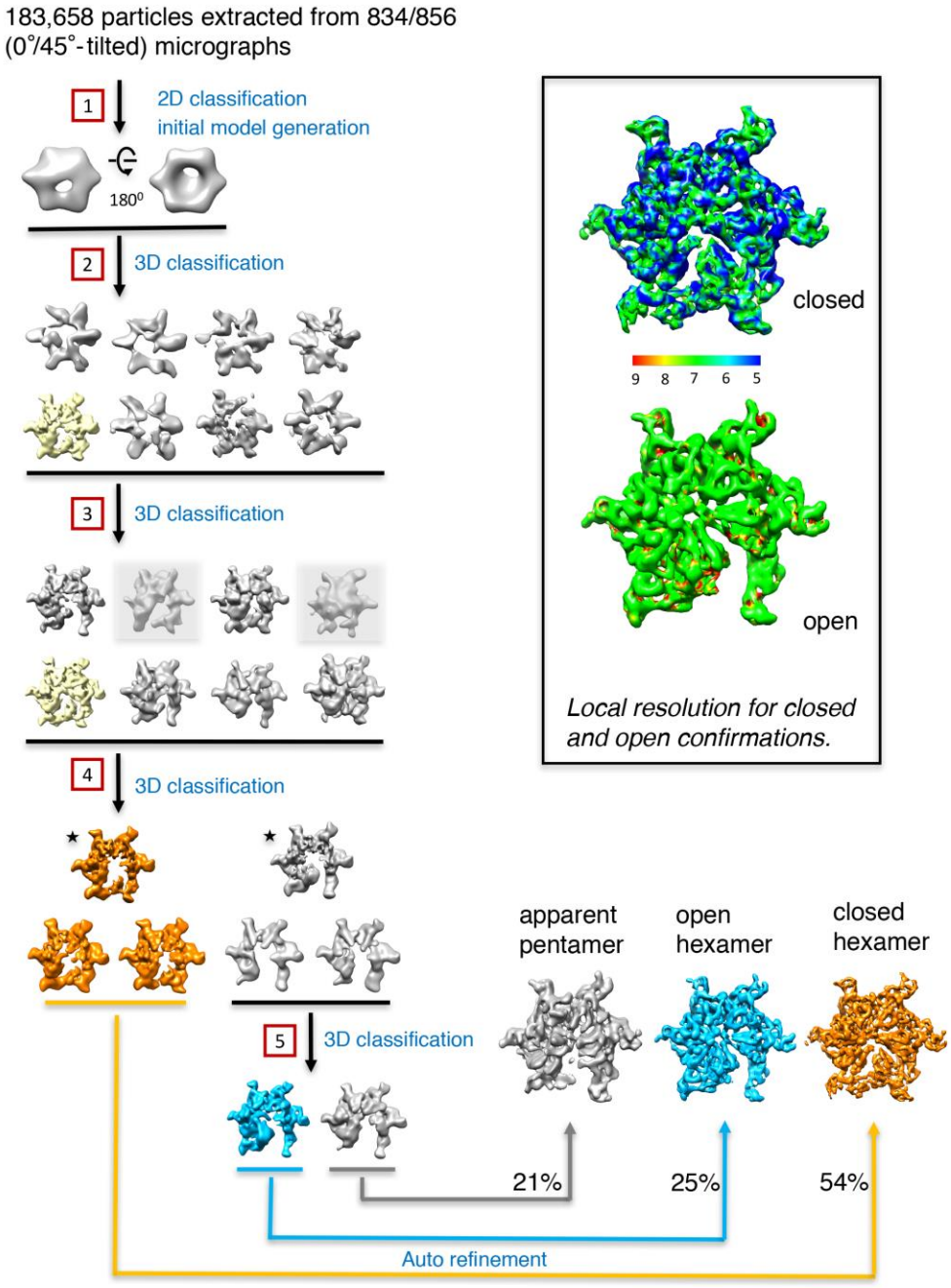

fig. S3. Flow chart of particle classification and 3D map reconstruction. Details are provided in the Methods section.

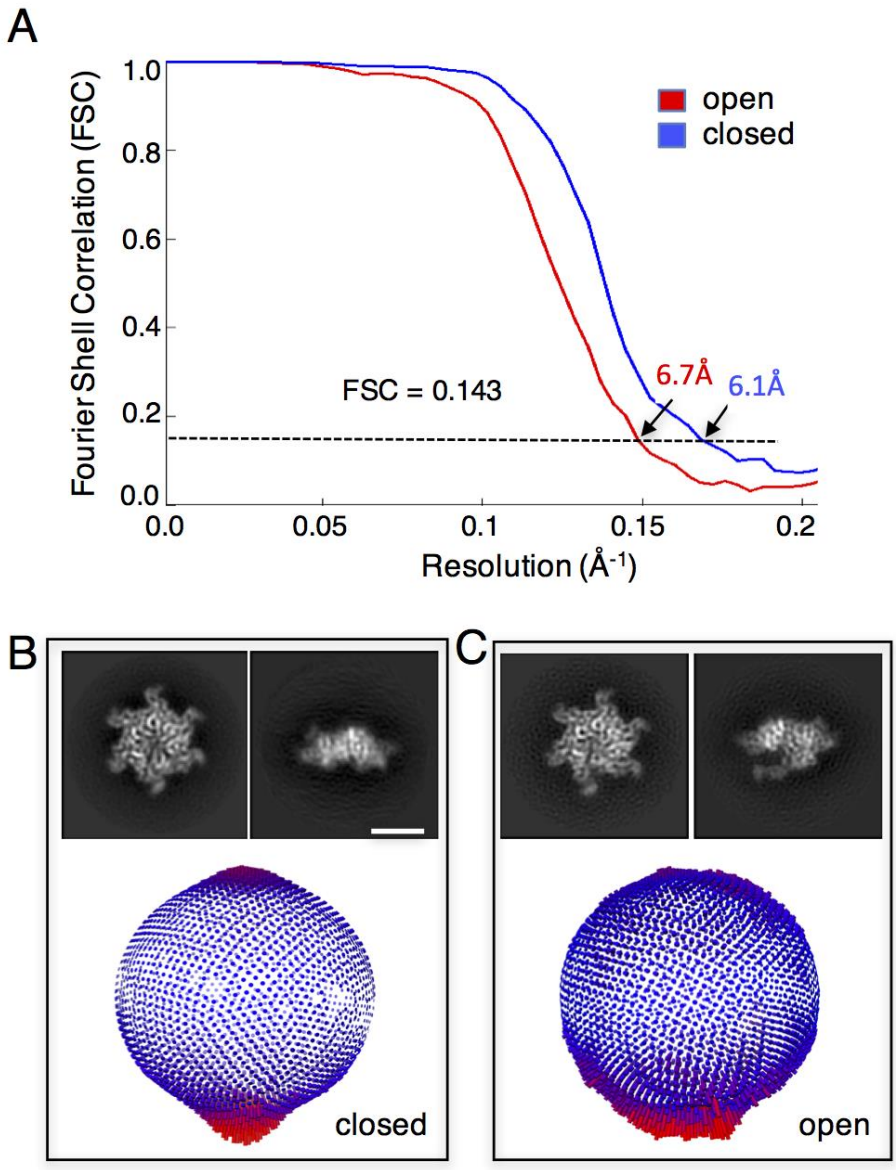

fig. S4. Map resolution estimation and projection angle distribution. (**A**) Gold standard Fourier Shell Correlation (FSC) curves for the final 3D maps of Vps4 indicate resolution of 6.1 Å and 6.7 Å for the closed and open conformers, respectively (FSC=0.143 criterion). (**B** and **C**) 3D map re-projection and Euler angle distribution for the closed (B) and open (C) conformers.

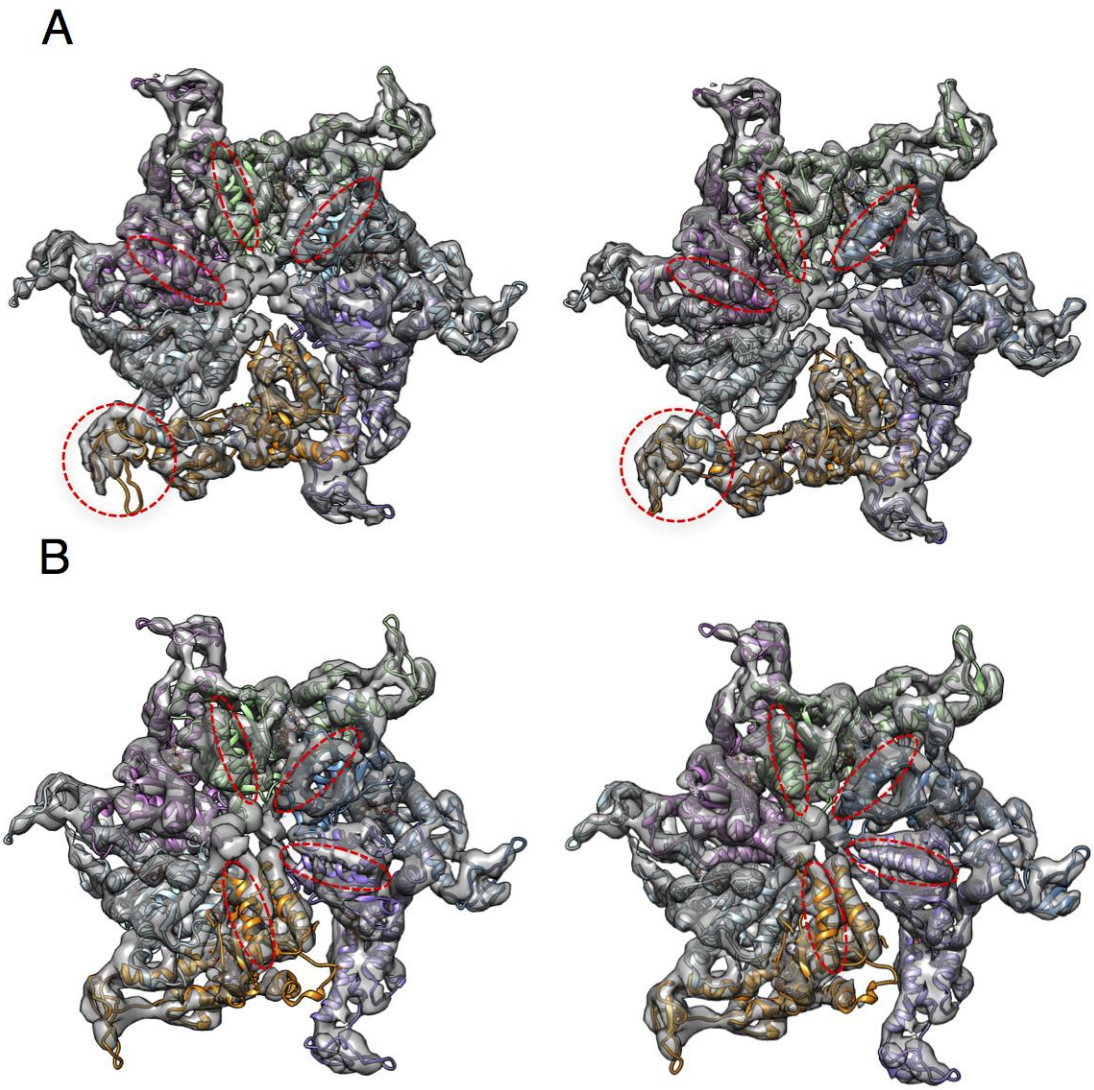

fig. S5. Fitting of the Vps4 hexamer structure into the cryo-EM map. (**A**) Closed conformation of Vps4 hexamer after rigid body fitting (left) and flexible fitting (right). The cross correlation coefficient between protein backbone and the cryo-EM map is 0.753 and 0.846, respectively. (**B**) Open conformation after rigid body fitting (left) and flexible fitting (right). The cross correlation coefficient is 0.800 and 0.886, respectively. The red dashed line circled regions in both (A) and (B) are sample regions whose fitting into the cryo-EM map is significantly improved by flexible fitting over rigid body fitting.

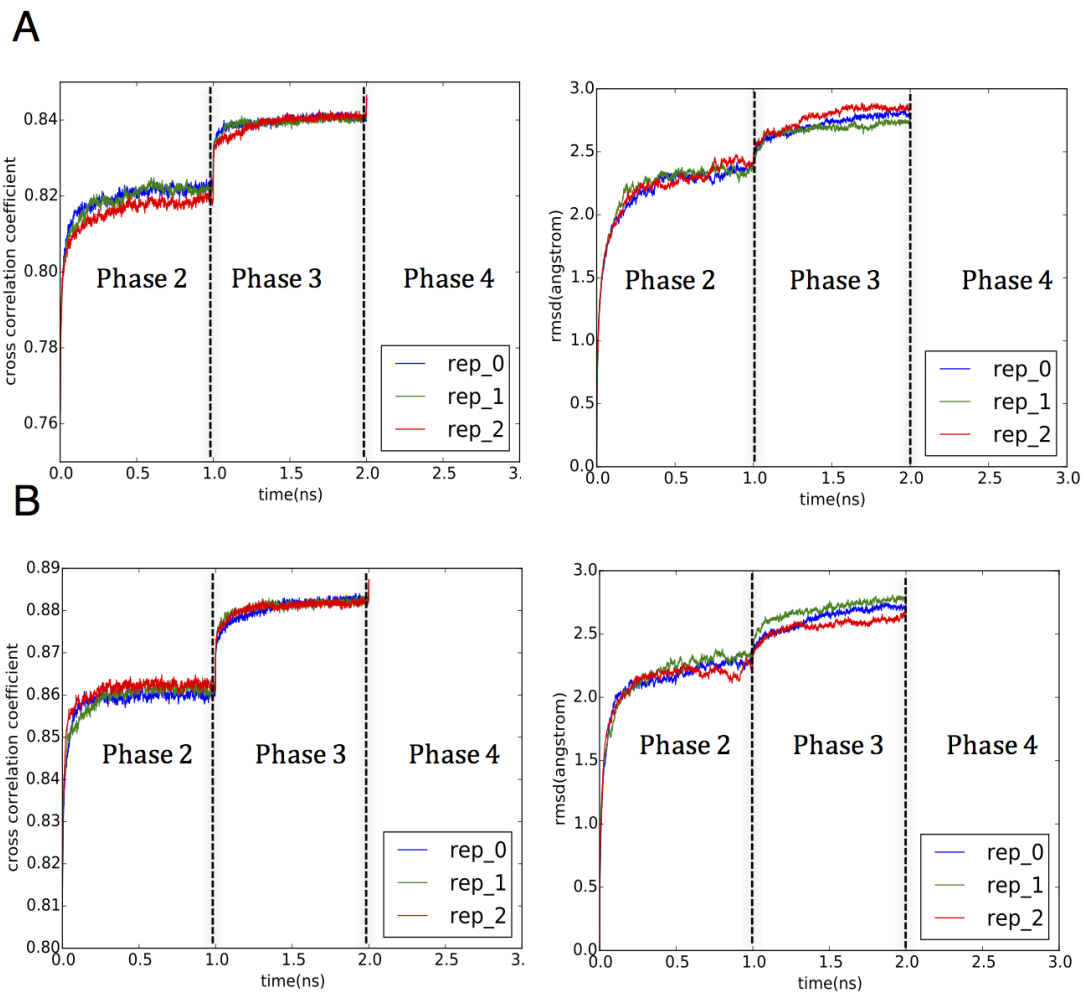

fig. S6. Molecular dynamics flexible fitting. (**A**) Left, cross correlation coefficient between the backbone protein structure and the cryo-EM map for the closed conformation throughout the last three phases of MDFF for each of the three replicate runs. Right, backbone root mean square deviation (RMSD) from the starting structure for the closed conformation during the last three phases of MDFF for each run. (**B**) The same as in (A) for the open conformation.

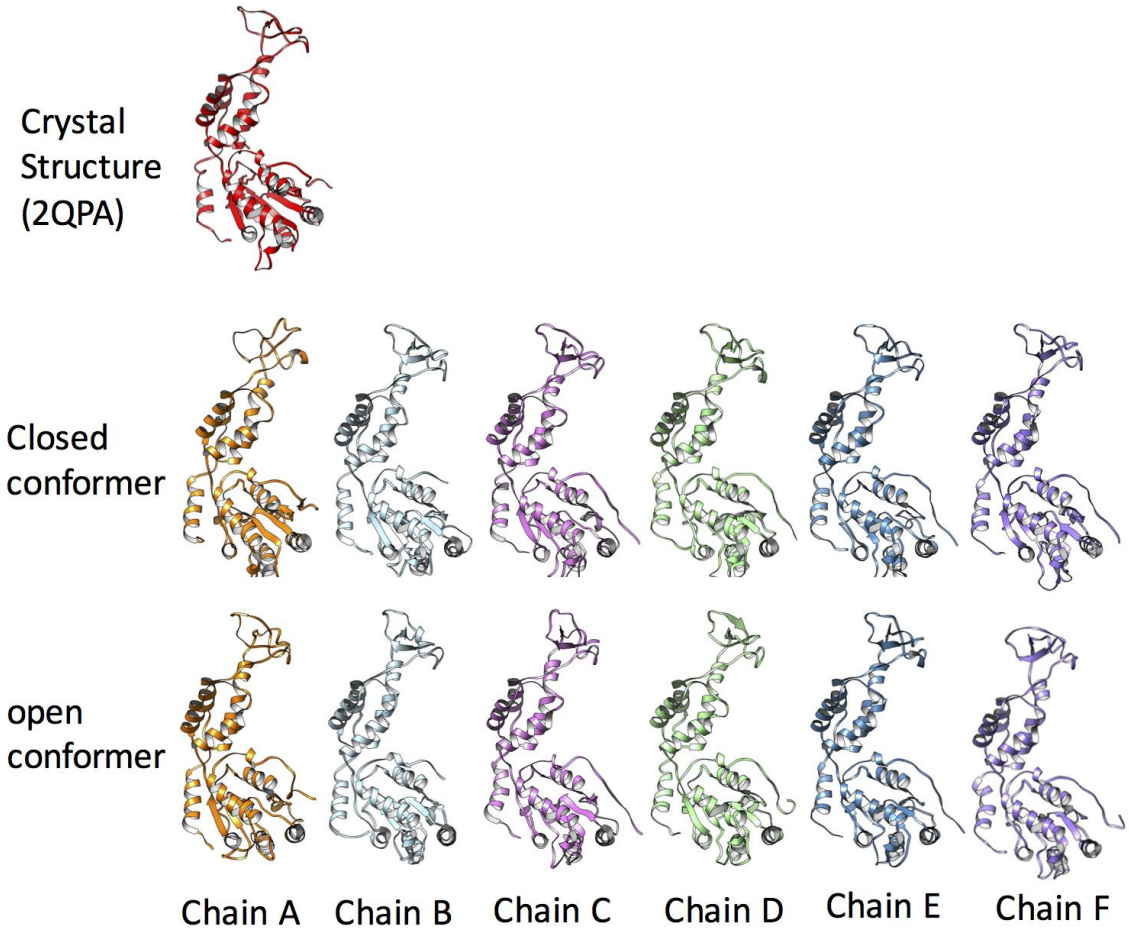

fig. S7. Comparison of the crystal structure and Vps4 hexamer subunit structures. Comparison between the crystal structure of Vps4 (2QPA, red) and MD-fitted subunit structures in the maps of closed and open hexamer conformers.

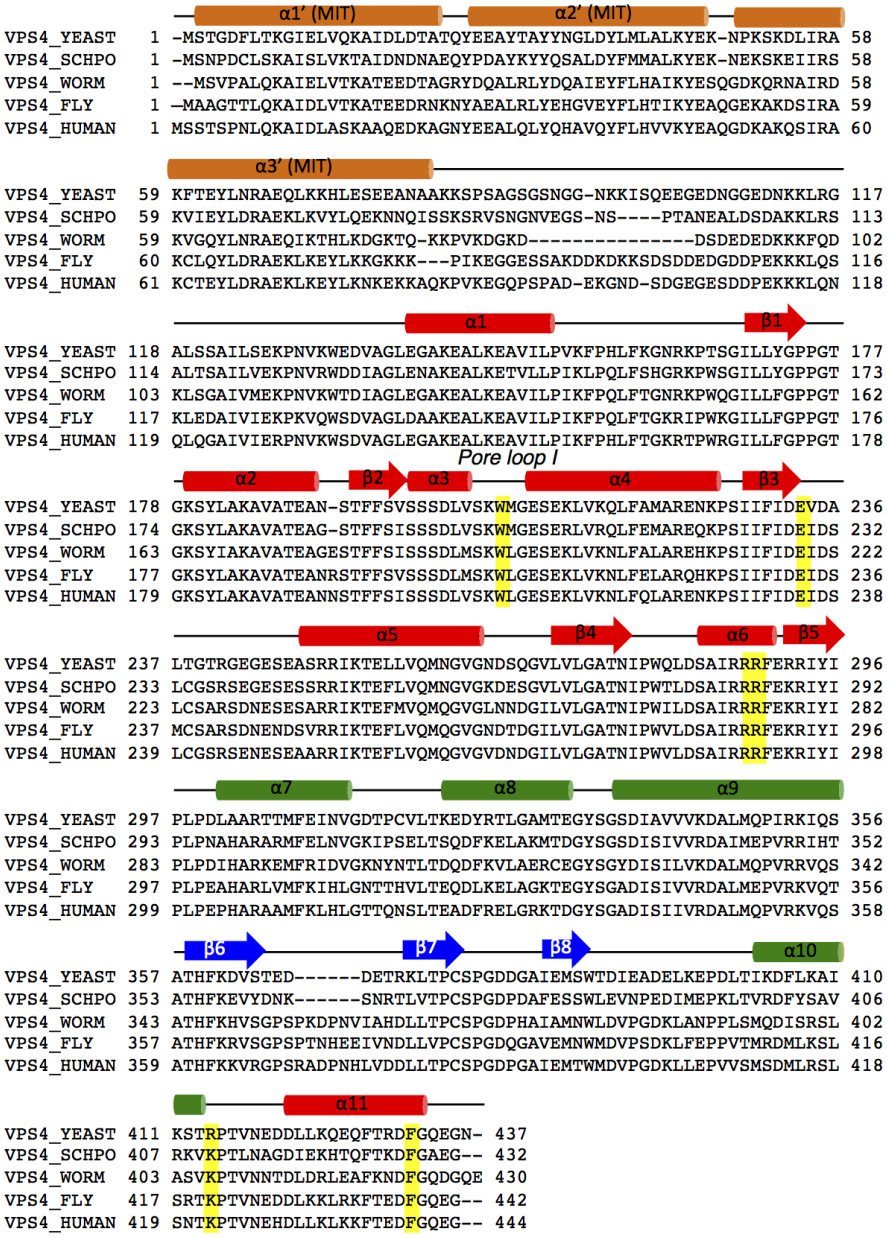

fig. S8. Sequence alignments of Vps4 proteins from *S. cerevisiae*, *Schizosaccharomyces pombe*, *Caenorhabditis elegans*, *Drosophila melanogaster*, and *Homo sapiens*. Secondary structural elements are shown above the sequences: α-helix, cylinder; β-strand, arrow; loop, line. The MIT domain is colored orange, large ATPase

domain is colored red, small ATPase domain is colored green and the β domain is colored blue. Residues Trp206, Glu233, Arg288, Arg289, Arg414 and Phe432 are highlighted by yellow boxes.

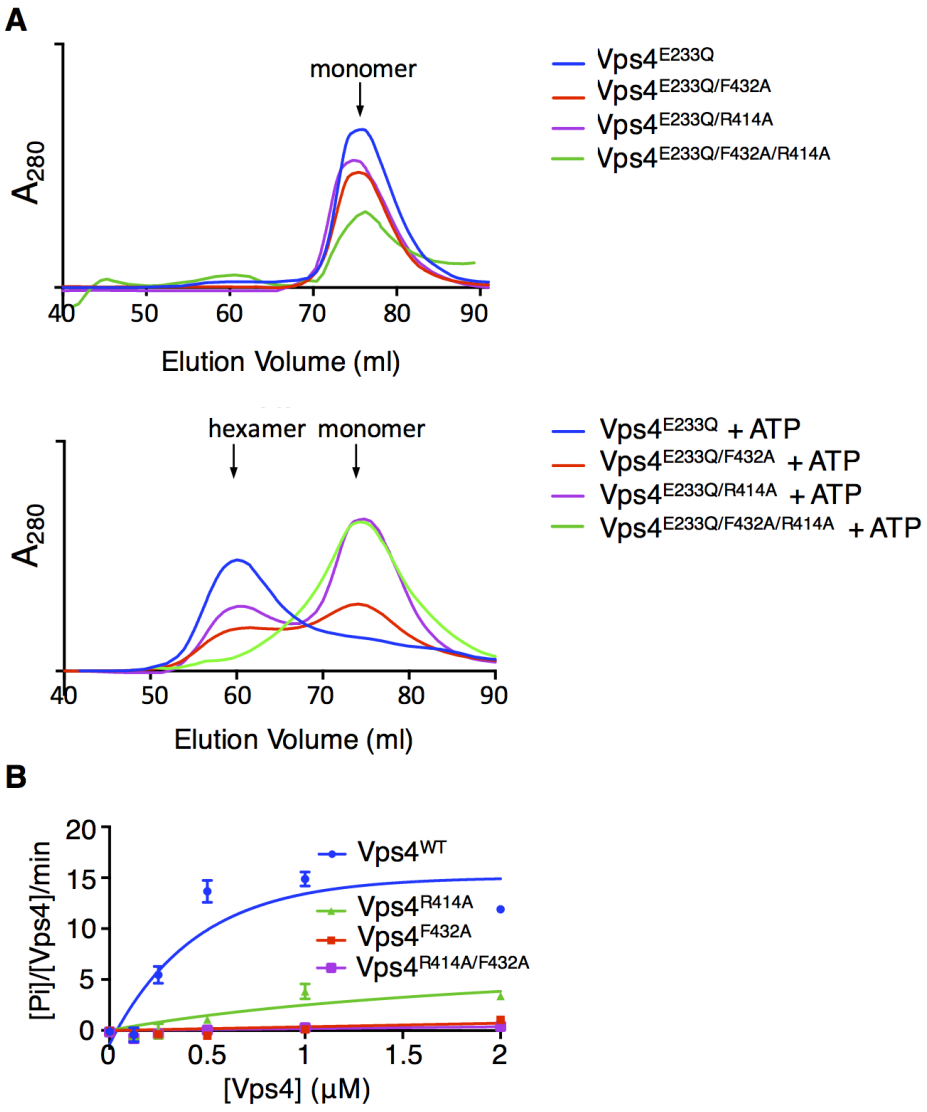

fig. S9. Residues at subunit interface III are important for Vps4 oligomerization and ATPase activity. (**A**) The oligomerization behavior of $Vps4^{E233Q}$, $Vps4^{E233Q/R414A}$, $Vps4^{E233Q/F432A}$, and $Vps4^{E233Q/R414A/F432A}$ was analyzed on a Superdex200 size exclusion column at a concentration of 30-50 μM. (**B**) ATPase activity of wild-type Vps4, $Vps4^{R414A}$, $Vps4^{F432A}$, and $Vps4^{R414A/F432A}$ were determined. Activity is expressed as μM inorganic phosphate released per μM Vps4 per min. Both single and double mutations result in dramatic decrease in activity.

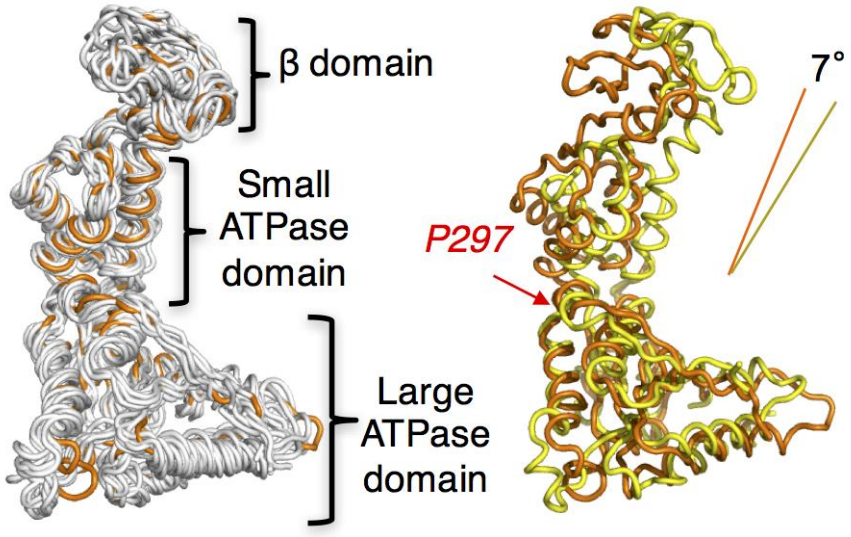

fig. S10. Structural comparison of Vps4 subunits in the open and closed conformations. Left, subunits B-F in both conformers (grey) are aligned with each other and against subunit A in the open conformer (orange). Right, subunit A in the closed conformer (yellow) is aligned against subunit A in the open conformer (orange). All alignments are based on the large ATPase domain.

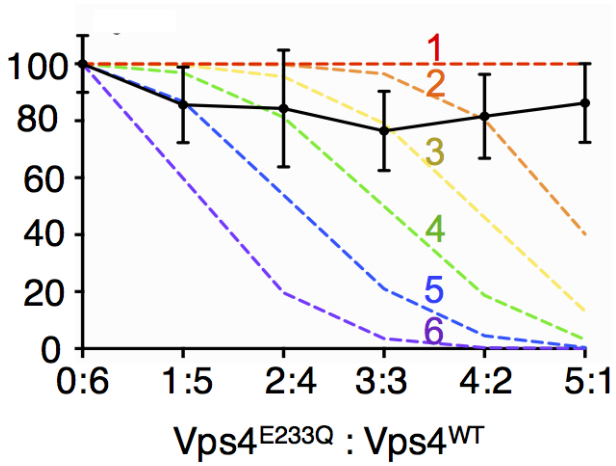

fig. S11. One wild-type subunit per hexamer is sufficient to maintain full Vps4 hexamer ATPase activity. $Vps4^{WT}$ and $Vps4^{E233Q}$ were mixed at different ratios with the total protein concentration fixed at 0.5 μM (solid line), and the ATPase activity was measured as μM inorganic phosphate released per μM of $Vps4^{WT}$ per min. The activity for 0.5 μM $Vps4^{WT}$ was set as 100%. The dashed lines represent theoretical activity curves if one, two, three, four, five, or six wild-type subunits are required to maintain Vps4 hexamer activity. The experimental curve is in agreement with the theoretical curve for which only 1 of 6 subunits is required for maximal ATPase activity.

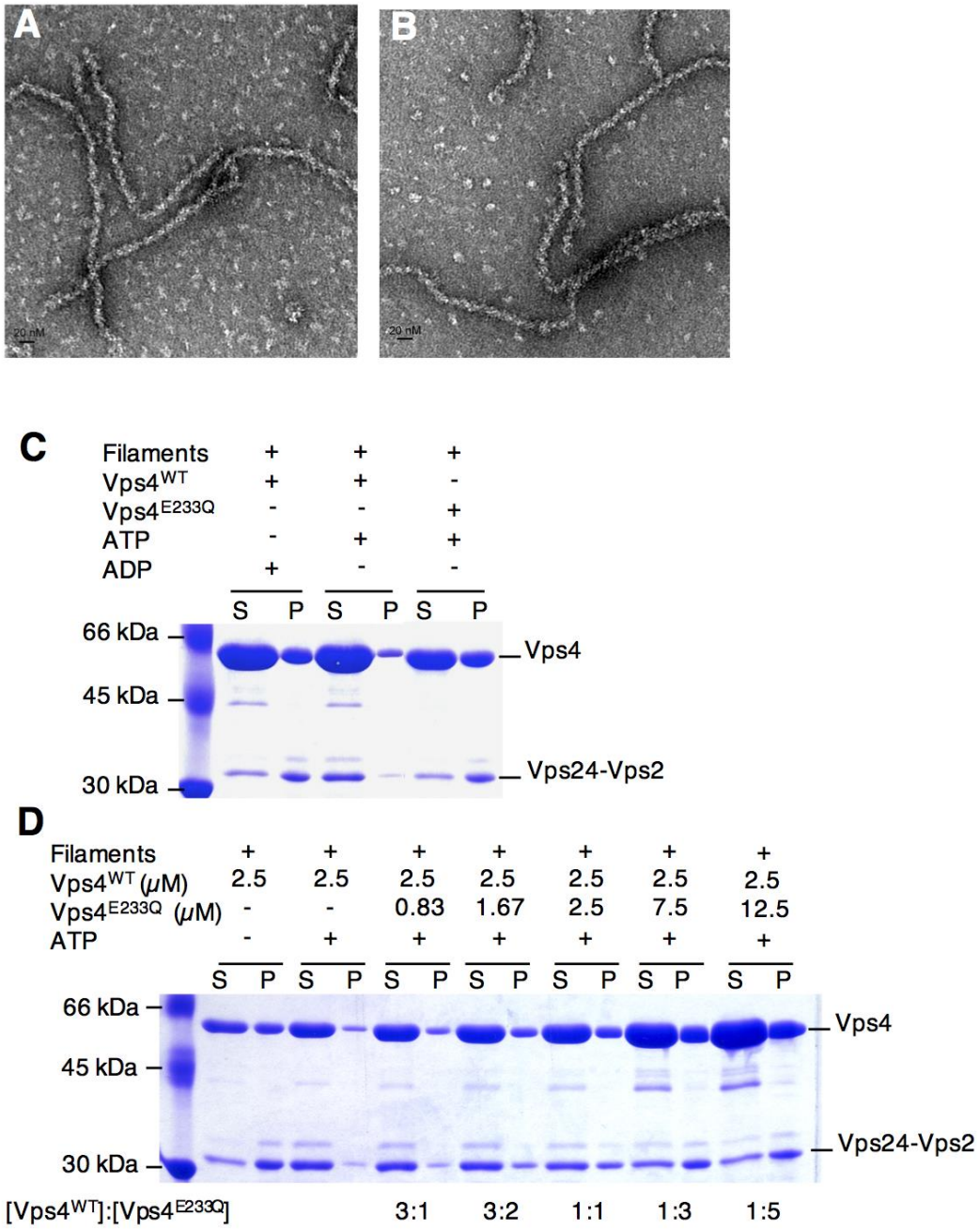

fig. S12. Filament disassembly activity of Vps4. (**A** and **B**) Electron micrographs of negative stained Vps24-Vps2 filaments after incubation with Vps4 and ADP (A) or $Vps4^{E233Q}$ and ADP (B) for 15 min on ice. Scale bars, 20 nm. (**C** and **D**) SDS-PAGE gel analysis of Vps4 mediated disassembly of Vps24-Vps2 filaments.